TUDelft

Delft University of Technology

Movement dynamics of divisome proteins and PBP2x

FtsW in cells of Streptococcus pneumoniae

Perez, Amilcar J.; Cesbron, Yann; Shaw, Sidney L.; Villicana, Jesus Bazan; Tsui, Ho Ching T.; Boersma, Michael J.; Ye, Ziyun A.; Tovpeko, Yanina; Dekker, Cees; More Authors

Important note
To cite this publication, please use the final published version (if applicable).
Please check the document version above.

Movement dynamics of divisome proteins and PBP2x: FtsW in cells of *Streptococcus pneumoniae*

Amilcar J. Perez[a], Yann Cesbron[b], Sidney L. Shaw[a], Jesus Bazan Villicana[a], Ho-Ching T. Tsui[a], Michael J. Boersma[a], Ziyun A. Ye[a], Yanina Tovpeko[a], Cees Dekker[c], Seamus Holden[b], and Malcolm E. Winkler[a,1]

[a]Department of Biology, Indiana University, Bloomington, IN 47405-7005; [b]Centre for Bacterial Cell Biology, Institute for Cell and Molecular Biosciences, Newcastle University, NE2 4AX Newcastle upon Tyne, United Kingdom; and [c]Department of Bionanoscience, Kavli Institute of Nanoscience Delft, Delft University of Technology, 2628 CD Delft, The Netherlands

Bacterial cell division and peptidoglycan (PG) synthesis are orchestrated by the coordinated dynamic movement of essential protein complexes. Recent studies show that bidirectional treadmilling of FtsZ filaments/bundles is tightly coupled to and limiting for both septal PG synthesis and septum closure in some bacteria, but not in others. Here we report the dynamics of FtsZ movement leading to septal and equatorial ring formation in the ovoid-shaped pathogen, *Streptococcus pneumoniae*. Conventional and single-molecule total internal reflection fluorescence microscopy (TIRFm) showed that nascent rings of FtsZ and its anchoring and stabilizing proteins FtsA and EzrA move out from mature septal rings coincident with MapZ rings early in cell division. This mode of continuous nascent ring movement contrasts with a failsafe streaming mechanism of FtsZ/FtsA/EzrA observed in a Δ*mapZ* mutant and another *Streptococcus* species. This analysis also provides several parameters of FtsZ treadmilling in nascent and mature rings, including treadmilling velocity in wild-type cells and *ftsZ*(GTPase) mutants, lifetimes of FtsZ subunits in filaments and of entire FtsZ filaments/bundles, and the processivity length of treadmilling of FtsZ filament/bundles. In addition, we delineated the motion of the septal PBP2x transpeptidase and its FtsW glycosyl transferase-binding partner relative to FtsZ treadmilling in *S. pneumoniae* cells. Five lines of evidence support the conclusion that movement of the bPBP2x:FtsW complex in septa depends on PG synthesis and not on FtsZ treadmilling. Together, these results support a model in which FtsZ dynamics and associations organize and distribute septal PG synthesis, but do not control its rate in *S. pneumoniae*.

TIRF microscopy | microhole vertical imaging | FtsZ treadmilling | nascent ring formation | PBP2x:FtsW shared dynamics

Cell division in most bacteria is mediated by the tubulin homolog, FtsZ, which polymerizes into dynamic filaments and bundles at the middle or toward the pole of dividing cells (1, 2). Polymerization of FtsZ filaments/bundles initiates sequential binding of a series of proteins that ultimately assemble into a controlled divisome machine for septal peptidoglycan (PG) synthesis leading to cell division (3, 4). The assembly of this machine involves the binding of FtsZ filaments to membrane-anchoring and filament-stabilizing and -bundling proteins (1). An ensemble of conserved FtsZ-ring component and regulator proteins then interact sequentially followed by a class B penicillin-binding protein [bPBP; transpeptidase (TP) of PG peptides], FtsW [glycosyl transferase (GT) that builds glycan chains], and MurJ (Lipid II substrate flippase) (5–7). The exact composition of FtsZ-ring divisomes, the mechanism of timing and triggering of septal PG synthesis, and the involvement of PG remodeling by hydrolases is only partly understood and varies widely among different bacterial species (8–10).

Biochemical work demonstrates that FtsZ filaments move directionally by a treadmilling mechanism, similar to that first found for eukaryotic tubulins (11). In treadmilling, FtsZ-GTP monomers add to the growing (+) end of advancing filaments, and FtsZ-GDP, produced by FtsZ-catalyzed GTP hydrolysis, dissociate from the other disappearing (−) end of the FtsZ filament (12). The net result is directional movement of filaments, in which central FtsZ-GTP subunits are stationary. Total internal reflection fluorescence microscopy (TIRFm) of moving FtsZ filaments/bundles and single-molecule (SM)-TIRFm experiments have recently established FtsZ treadmilling in the Gram-positive and -negative rod-shaped bacteria, *Bacillus subtilis* and *Escherichia coli*, respectively (12, 13). In these studies, the velocity of filaments/bundles was shown to depend on the FtsZ GTPase activity, but was independent of the addition of TP-inhibiting antibiotics. Both studies also concluded that bidirectional treadmilling of FtsZ filaments/bundles plays a role in organizing and distributing the septal PG synthesis apparatus. In *B. subtilis*, treadmilling is tightly coupled to and limiting for septal PG synthesis and septum closure, such that the velocity of septal bPBP2b movement correlates with the velocity of treadmilling of FtsZ filaments/bundles (12). This mode of PBP movement differs from that of MreB-mediated sidewall elongation that depends on PG synthesis and is blocked by antibiotics in *B. subtilis* and other rod-shaped bacteria (14, 15). Similarly, the velocities of bPBP3 (FtsI) and FtsZ treadmilling are correlated in *E. coli*, but curiously, treadmilling velocity does not limit the rate of septal PG synthesis determined by incorporation of fluorescent D-amino acids (FDAAs) or the rate of septum closure (13). In contrast, after septal PG synthesis is initiated in *Staphylococcus aureus*, cytokinesis to close the septum does not depend on FtsZ treadmilling and is likely driven by PG synthesis (16).

Compared with these model rod-shaped and spherical bacteria, much less is known about FtsZ ring dynamics in ovoid-shaped

Significance

This study answers two long-standing questions about FtsZ dynamics and its relationship to septal peptidoglycan (PG) synthesis in *Streptococcus pneumoniae*. In previous models, FtsZ concertedly moves from midcell septa to MapZ rings that have reached the equators of daughter cells. Instead, the results presented here show that FtsZ, FtsA, and EzrA filaments/bundles move continuously out from early septa as part of MapZ rings. In addition, this study establishes that the movement of bPBP2x:FtsW complexes in septal PG synthesis depends on and likely mirrors new PG synthesis and is not correlated with the treadmilling of FtsZ filaments/bundles. These findings are consistent with a mechanism where septal FtsZ rings organize directional movement of bPBP2x:FtsW complexes dependent upon PG substrate availability.

MICROBIOLOGY

bacteria, such as the human respiratory pathogen, *Streptococcus pneumoniae* (pneumococcus). Newly divided ovococcus bacteria form prolate ellipsoid-shaped cells containing equatorial rings composed of FtsZ and other proteins (*SI Appendix*, Fig. S1*A*, *Bottom*) (17, 18). These equatorial rings become the mature septa at the start of division (19, 20). Mature FtsZ rings contain all of the proteins required for the stabilization and placement of FtsZ protofilaments and for PG synthesis during the next round of division (21). *S. pneumoniae* lacks conventional nucleoid occlusion mechanisms, and high-resolution microscopy shows that FtsZ protofilaments are distributed in nodal patterns around mature septal FtsZ rings that surround the undivided nucleoid marked by its origin of replication (*SI Appendix*, Fig. S1*A*, *Bottom*) (22–24).

To construct an ellipsoid shape, two modes of PG synthesis are organized by the septal FtsZ rings in *S. pneumoniae* (25). Septal PG synthesis mediated by class B PBP2x (bPBP2x) and other proteins closes inward to separate cells, whereas peripheral PG synthesis mediated by bPBP2b and other proteins emanates outward from midcells to elongate cells (*SI Appendix*, Fig. S1*A*, *Top*). Early in division, a ring composed of MapZ (LocZ) splits (*SI Appendix*, Fig. S1) and is moved by peripheral PG synthesis toward the equators of the daughter cells (26, 27), preceded by the origin of replication (*SI Appendix*, Fig. S1*A*, *Top*) (23). MapZ movement precedes migration of FtsZ, FtsA [FtsZ membrane anchor and peripheral PG regulator in *S. pneumoniae* (20)], and EzrA [FtsZ assembly modulator in *B. subtilis* (28) and FtsZ assembly positive regulator in *S. pneumoniae*] to the equators (*SI Appendix*, Fig. S4 *B–F*). During middle-to-late cell division, FtsZ, EzrA, and FtsA are observed at the closing septum as well as at both developing equators, resulting in a distinctive three-band pattern (*SI Appendix*, Fig. S1*A*, *Middle* and *SI Appendix*, Figs. S3*A* and S4 *B–F*). After FtsZ, EzrA, and FtsA relocate to equators, proteins involved in PG synthesis, including DivIVA (negative-curvature binding protein that determines cell shape) (29), MltG (endo-lytic transglycosylase in peripheral PG synthesis) (30), GpsB (regulator that distributes septal and peripheral PG synthesis) (31), StkP (Ser/Thr protein kinase that regulates PG synthesis) (32), and bPBP2x (19) remain at the septum and migrate to equators right before cells divide (*SI Appendix*, Fig. S4 *G–L*).

Little is known about how FtsZ moves from the septum to the MapZ rings that have arrived near the equators of daughter cells. Current models postulate that FtsZ migrates *en masse* from the septum to the equatorial MapZ rings at a later stage in division (e.g., ref. 23). A recent study used TIRFm to demonstrate treadmilling of FtsZ filaments/bundles in equatorial rings of *Streptococcus mutans* (33), which is evolutionarily distant from *S. pneumoniae* (33). In this study, *en masse* streaming of FtsZ from septa to equatorial rings was detected in a minority (~7%) of dividing *S. mutans* cells (33). Here, we show that key proteins involved in FtsZ ring assembly and in septal and peripheral PG synthesis have different dynamics during pneumococcal cell division. We demonstrate and describe several parameters of FtsZ treadmilling in *S. pneumoniae*. Furthermore, we report that nascent rings containing FtsZ, FtsA, and EzrA move out from mature septa guided by MapZ throughout the cell cycle. Streaming of EzrA was only observed in Δ*mapZ* mutants as a possible division failsafe mechanism. In contrast, several other proteins were confined to mature septa and showed little dynamic movement within the limits of conventional TIRFm. Finally, we show that bPBP2x interacts with FtsW and that both proteins show directional movement along mature septal rings, independent of FtsZ treadmilling. Together, these findings reveal aspects about the movement and assembly of FtsZ/FtsA/EzrA filament/bundles in dividing *S. pneumoniae* cells and show that septal bPBP2x: FtsW complexes require PG synthesis for movement.

Results

Relocation of *S. pneumoniae* Cell Division and PG Synthesis Proteins Occurs in Three Stages and Is Dependent on pH.

To compare the dynamics of pneumococcal cell division and PG synthesis proteins, we constructed and vetted a large set of fluorescent and

HaloTag (HT) protein fusions expressed from single-copy genes at their native chromosome loci (*SI Appendix*, Table S1). Each protein fusion contains a linker region specified in *SI Appendix*, Table S1, but omitted in the text and figures to simplify designations. An unencapsulated derivative (Δ*cps*) of serotype 2 strain D39 was used for these studies, because encapsulated D39 forms short chains (*SI Appendix*, Fig. S1*A*) that make microscopy more difficult, and capsule tends to mask morphology defects of constructs (34). None of the final fluorescent- and HT–protein fusions ostensibly altered growth or cell morphology, and each showed localization of labeled proteins at septa and new equators of dividing cells grown exponentially in C+Y liquid medium, pH 6.9 (5% CO_2) (*SI Appendix*, Figs. S2 and S3), consistent with previous localization studies (see below).

Demographs generated by MicrobeJ (35) from fields of exponentially growing cells supported and extended the conclusion that *S. pneumoniae* division and PG synthesis proteins relocate from the septa of single, early divisional cells (left side of demographs) to the equators of new daughter cells (right side of demographs) in three distinct stages (*SI Appendix*, Figs. S2*H* and S4). MapZ relocates early, before FtsZ, FtsA, and EzrA (23, 26, 27). Residual MapZ remained between new equatorial rings until the migration of FtsZ and its associated proteins, FtsA and EzrA (*SI Appendix*, Fig. S4 *A–F*), but a third septal ring of MapZ reported previously (26) was not detected in cells grown under these conditions (see also refs. 23 and 27). FtsZ, FtsA, and EzrA next relocate to new equators at approximately the same time, with residual EzrA and FtsA remaining at septa when most of FtsZ has migrated (*SI Appendix*, Fig. S4 *A–F*). Other cell division and PG synthesis proteins—including DivIVA, MltG, GpsB, StkP, bPBP2x, and FtsW—remain at septa after most FtsZ, FtsA, and EzrA have departed and move to the equators of daughter cells late in the division cycle (*SI Appendix*, Figs. S2*G* and S4 *J–L*) (21, 22, 29, 30, 32). The localization of StkP, bPBP2x, and FtsW is more diffuse away from septal and equatorial rings than that of the other proteins examined throughout the cell cycle (*SI Appendix*, Figs. S2*G* and S4 *J–L*). Western blot control experiments did not detect cleavage of the GFP or HT reporter domains from GFP-StkP and HT-bPBP2x (*SI Appendix*, Fig. S5). As shown later, diffusiveness in demographs corresponds to diffuse movement detected by TIRFm.

During these experiments, we unexpectedly noticed that the size and shape of wild-type Δ*cps* cells depends on pH in C+Y liquid medium. At pH ~7.6 (5% CO_2), which supports natural competence (36), pneumococcal cells are markedly longer and larger than at pH ~6.9 (5% CO_2), which is the physiological pH at the surface of epithelial cells in the human respiratory tract (*SI Appendix*, Fig. S6 *A* and *B*) (37). Underscoring the effects of higher pH, strains expressing GpsB-sfGFP or the GFP-StkP showed morphological defects characteristic of reduced GpsB or StkP function, respectively, in C+Y at pH 7.6, but not at pH 6.9 (*SI Appendix*, Figs. S2 and S6). Effects of pH on cell length and aspect ratio of wild-type cells were not observed in brain–heart infusion (BHI) broth (*SI Appendix*, Fig. S6*A*), which we used in previous studies but cannot be used here because of autofluorescence.

Dynamics of FtsZ in Nascent Rings That Form Parallel to Mature FtsZ Septal Rings.

TIRFm and epifluorescence microscopy showed that FtsZ filament motion was detected both inside and outside of mature septal rings in *E. coli* (13, 38) and *B. subtilis* cells (12). To determine the patterns of FtsZ movement in *S. pneumoniae* cells, we performed comparable TIRFm, which limits illumination to a 100- to 150-nm slice and removes out-of-focus background fluorescence light (39). TIRFm of cells was performed on agarose pads containing C+Y, pH 7.1 (no CO_2). Newly separated pneumococcal cells contain a mature midcell septal ring that appears as a prominent fluorescent band composed of multiple overlapping FtsZ filaments (Fig. 1 *A* and *B*). FtsZ filament/bundle motion is detected by fluctuations in kymographs of TIRFm images (*SI Appendix*, Fig. S7 *A* and *B*), but it was not possible to reliably
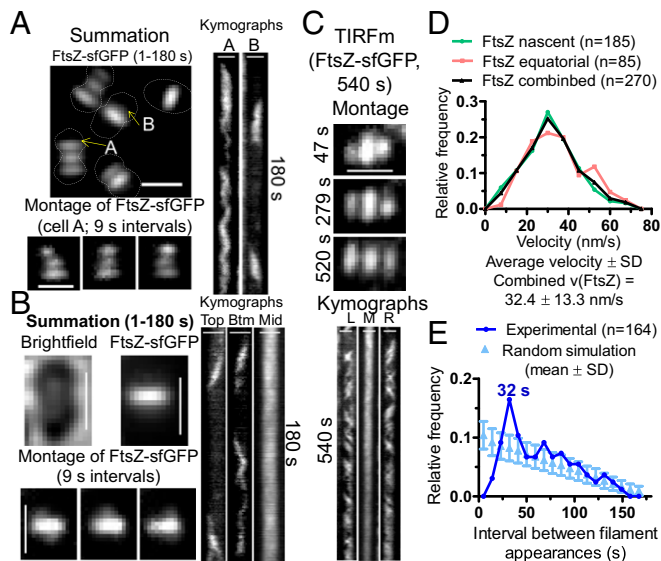
Fig. 1. FtsZ filament dynamics in nascent and early equatorial rings determined by TIRFm of strain IU9985 expressing FtsZ-sfGFP. Representative data are shown from two to four independent biological replicates. (*A*) Summation of frames from 180-s TIRFm movies of FtsZ-sfGFP (at one frame per second). Montage of images at 9-s intervals of the cell containing the indicated "A" ring in summation. (*Right*) Kymographs from 1 to 180 s; top equatorial "A" ring of cell in summation; area marked "B" above septal ring in summation. The dotted lines are approximate outlines of cell shape. (*B*) Summation of frames from 180-s movies of bright-field images of cells and TIRFm images of FtsZ-sfGFP of mature-septal and nascent rings. Montage of images at 9-s intervals shows FtsZ-sfGFP in nascent rings above and below mature-septal ring (Movies S1 and S2). (*Right*) Kymographs show FtsZ-sfGFP movement in the top nascent ring plane, bottom (Btm) nascent ring plane, and middle (Mid) mature-septal plane. (*C*) TIRFm movie taken over 540 s of a single cell. Montage shows frames of FtsZ-sfGFP in two nascent rings and the middle mature-septal FtsZ ring at the times indicated. Kymographs of the left (L) and right (R) nascent rings and the middle (M) mature-septal ring over the 540 s (9 min) are shown. (Scale bars in *A–C*, 1.0 μm.) (*D*) Distribution of velocities of FtsZ filaments/bundles in nascent rings, early equatorial rings, and the combination of nascent and equatorial rings. Velocities of FtsZ filament/bundles were binned in intervals of 7.5 nm/s. (*E*) Distribution of times of reappearance of FtsZ filaments/bundles moving in the same direction in nascent and early equatorial rings. Reappearance times were determined as described in *SI Appendix, Experimental Procedures* from four independent biological replicate experiments (*n* = 164 events) and are binned in 9-s intervals (dark blue). A simulation (light blue) of the means ± SDs of random events for each reappearance interval in kymographs of 1–180 s was generated as described in *SI Appendix, Experimental Procedures*. The reappearance interval of FtsZ filaments/bundles matched the random simulation within 2 SDs, except at 32 s, which showed a significant difference (see *Dynamics of FtsZ in Nascent Rings That Form Parallel to Mature FtsZ Septal Rings*).

quantitate FtsZ filament/bundle velocities by TIRFm in densely packed mature septal rings (Fig. 1 *B* and *C* and Movie S1). FtsZ filament/bundle speeds in mature septal rings were determined by wide-field imaging of vertically oriented cells, as described below.

We detected the initial stages of formation of nascent FtsZ rings on either side of mature septal rings (Fig. 1 *A–C*). FtsZ in nascent rings was detected as oblong spots moving in both directions parallel to mature septal rings (Fig. 1 *A–C* and Movie S2). Nascent FtsZ rings first appear very close to mature septal rings, and this distance increases as the nascent FtsZ filaments move outward toward the equators of daughter cells, eventually resulting in the characteristic pattern of three parallel FtsZ rings in mid-to-late divisional *S. pneumoniae* cells (Fig. 1 *A* and *C*). Summations of TIRFm images taken over 180-s movies indicate that the diameters of nascent rings start out approximately equal to those of mature septal rings (Fig. 1 *A* and *C*). Kymographs through the long axis of cells show that nascent FtsZ rings form asynchronously on both sides of mature septal rings, with one

nascent FtsZ ring detected slightly before the other ∼50% of the time (e.g., Fig. 2*A*). We confirmed that this outward movement was not specific to FtsZ-sfGFP by using other FtsZ-tagged constructs (*SI Appendix*, Fig. S8). Nascent FtsZ rings move away from septal rings, add more filaments/bundles, and develop into early equatorial rings, in which directional velocities of FtsZ filaments/bundles are still detected (A in Fig. 1*A* and Fig. 2*B*). The diameters of equatorial rings became larger than those of residual septal rings, and the number of overlapping FtsZ filaments/bundles within new equatorial rings continue to increase (Figs. 1*A* and 2*A*). As the density of FtsZ filaments/bundles increases in new equatorial rings, motion is indicated by fluctuations in TIRFm kymographs (Fig. 1*C*, *SI Appendix*, Fig. S7*E*, and Movies S1 and S2). We show below that there is a correspondence between the position of nascent rings of FtsZ, FtsA, and EzrA and movement of the MapZ protein ring out from mature septal rings to the new equatorial rings of daughter cells.

Velocities of *S. pneumoniae* FtsZ-sfGFP filaments/bundles moving in either direction in nascent rings were determined from kymographs (Fig. 1 *A–D* and *SI Appendix*, Fig. S9*A*). FtsZ filament velocities were similar in nascent (31.5 ± 13.0 nm/s; average ± SD) and early equatorial rings (34.4 ± 13.7 nm/s), with a combined average FtsZ filament velocity of 32.4 ± 13.3 nm/s in cells in C+Y, pH 7.1 (no CO_2) (Fig. 1 *A–D*). FtsZ filament velocities were comparable in cells in C+Y, pH 7.8 medium (no CO_2) (33.0 ± 10.0 nm/s) (*SI Appendix*, Fig. S6*D*). The velocities of *S. pneumoniae* FtsZ filaments are similar to those reported previously for FtsZ filament/bundle movement in septal rings of *E. coli* (27.8 ± 17.1 nm/s) (13) and *B. subtilis* (32 ± 7.8 nm/s) (12). Other tags [-GFP or i-tag-HT (iHT)] on *S. pneumoniae* FtsZ resulted in a filament/bundle velocity of ∼32 nm/s, similar to that of FtsZ-sfGFP, with the exception of FtsZ-HT, which moved about 28% faster at ∼41 nm/s (*SI Appendix*, Fig. S9*B*). Of these constructs, FtsZ-sfGFP is the most functional, as this fusion causes minimal synthetic defects when combined with Δ*mapZ* (*SI Appendix*, Fig. S9*C*), similar to FtsZ-CFP published previously (23). We also analyzed the time between FtsZ-sfGFP filament appearances moving in the same direction (Fig. 1*E*). The relative frequency of appearance of FtsZ filaments moving in the same direction for the most part followed a random distribution,
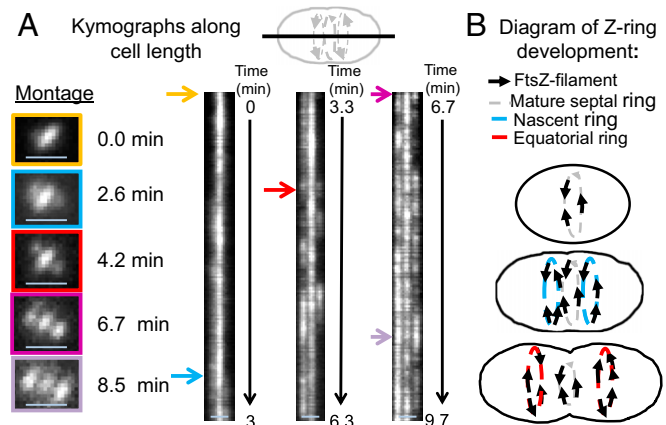
Fig. 2. Development of nascent rings into equatorial rings of daughter cells revealed by kymographs along the cell length. TIRFm was performed to track FtsZ-sfGFP in strain IU9985 for long periods of time (9.7 min, at one frame per second) as described in *SI Appendix, Experimental Procedures*. (*A*) Asynchronous formation of nascent FtsZ-rings tracked by kymographs taken along the long axis of the cell. Colored arrows correspond to the times individual cells were imaged for the montage. Nascent rings formation was asynchronous in ∼50% of cells. (Scale bars, 1 μm.) (*B*) Cartoon of the continuous outward movement of nascent FtsZ rings from mature septal rings during the first stages of *S. pneumoniae* cell division. See *Dynamics of FtsZ in Nascent Rings That Form Parallel to Mature FtsZ Septal Rings* for additional details.

except between 28 and 37 s (Fig. 1E). The diameter of FtsZ-sfGFP rings in these live pneumococcal cells was determined by 2D-deconvolution epifluorescence microscopy to be 0.80 ± 0.06 μm, which corresponds to a circumference of $\sim 2,500$ nm. Thus, the frequency of FtsZ filament appearance at intervals of 28–37 s (peak at 32 s) cannot be caused by circumferential periodicity of FtsZ filaments moving at ~ 32 nm/s, but may be related to an average clocked initiation of new FtsZ filaments.

FtsZ Filament/Bundle Dynamics and Processivity in Mature Septal Rings. To determine the speed, processivity, and lifetime of FtsZ filaments/bundles in mature septal rings, individual *S. pneumoniae* cells expressing FtsZ-sfGFP were oriented vertically in a microhole device described previously (Fig. 3A and *SI Appendix*, Fig. S10) (12). FtsZ movement in the imaging plane was recorded by wide-field time-lapse microscopy of mature septal rings with a range of diameters (Fig. 3A, *SI Appendix*, Fig. S11, and Movie S3). Images were denoised, and kymographs were generated (*Experimental Procedures* and *SI Appendix*, Fig. S10) (12). Lengths and angles of ~ 600 FtsZ filament tracks from 29 cells were quantitated and used to compute FtsZ filament/bundle speeds, processivity, and lifetimes (Fig. 3 B–D). FtsZ filament/bundles move bidirectionally around *S. pneumoniae* mature septal rings at an average speed of 30.5 ± 9.3 nm/s, which is comparable to the average velocity of FtsZ filaments/bundles in nascent and new equatorial rings (32.4 ± 13.3 nm/s) (Fig. 1D) and independent of cell diameter (*SI Appendix*, Fig. S11B). We conclude that the dynamic properties of FtsZ filaments/bundles in nascent and early equatorial rings match those of FtsZ filaments/bundles in mature septal rings. We also measured the total distance traveled by FtsZ filaments/bundles within septa. This gives a processivity distribution with an average of 515 ± 331 nm (Fig. 3C), meaning that an FtsZ filament typically traverses about one-fifth of the circumference of an *S. pneumoniae* cell. Related to processivity, the time that FtsZ filaments/bundles exist in tracks is distributed with an average of 17.1 ± 9.4 s (Fig. 3D).
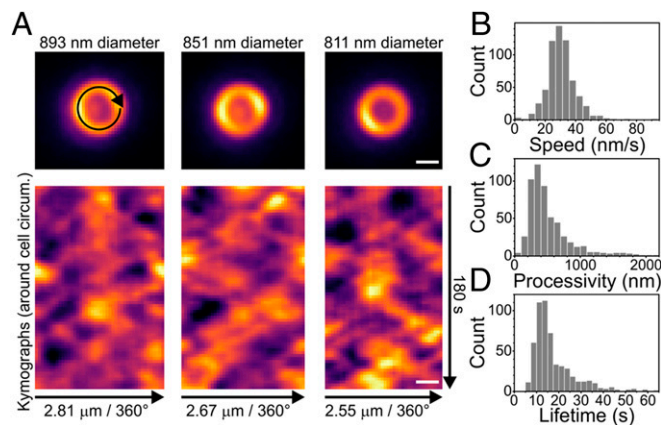
Fig. 3. FtsZ moves bidirectionally around the mature-septal division plane with filament/bundle velocities similar to those determined in nascent FtsZ rings. IU9985 cells expressing FtsZ-sfGFP were immobilized vertically, and FtsZ-sfGFP dynamics (Movie S3) was determined as described in *SI Appendix, Experimental Procedures*. (*A, Upper*) Representative snapshot images of FtsZ-sfGFP septal rings with typical diameters used in analyses. Images in *SI Appendix*, Fig. S11 illustrate the range of cell diameters observed. (*Lower*) Kymographs around cell circumference showing multiple FtsZ-sfGFP filaments/bundles treadmilling in both directions. Time-lapse images of the ring circumference were unwrapped into lines (black arrow, *Upper Left*) to generate the kymograph rows. (Scale bars, 500 nm.) (*B–D*) Individual filament/bundle tracks in kymographs were quantified from 29 cells (*SI Appendix*, Fig. S10) to give distributions of FtsZ-sfGFP filament treadmilling speed (*B; n = 605*), processivity (*C; n = 544*), and lifetime (*D; n = 544*). Mean ± SD; speed = 30.5 ± 9.3 nm/s; processivity = 515 ± 544 nm; lifetime = 17.1 ± 9.4 s.
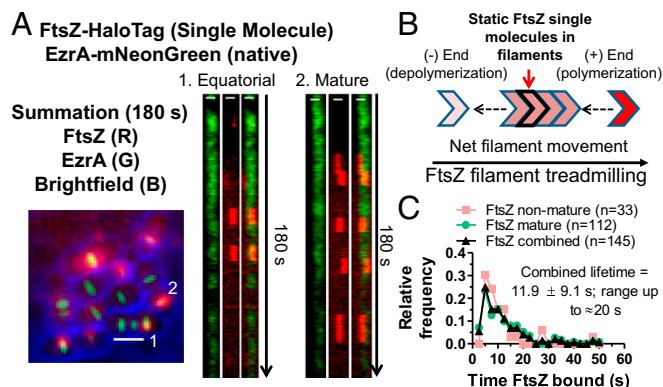
Fig. 4. Treadmilling of FtsZ filaments/bundles in mature and equatorial rings. (*A*) Strain IU14352 expressing FtsZ-HT EzrA-mNG was grown in C+Y, pH 6.9 at 37 °C in 5% CO_2 to $OD_{620} \sim 0.1$, and SM-TIRFm of FtsZ-HT labeled with JF549 HT ligand was performed as described in *SI Appendix, Experimental Procedures*. (Scale bars in summation, 1.0 μm.) (*Left*) Overlaid summation of images from 180-s movie (at one frame per second) for bright-field (blue), EzrA-mNG (green), and FtsZ-HT-JF549 (red). (*Right*) Kymographs from 1 to 180 s of rings indicated in the summation. (Scale bars in kymographs, 0.5 μm.) Data are representative from two independent biological replicates in which >60 cells were analyzed (Movie S4). (*B*) Diagram of FtsZ filament movement by a treadmilling mechanism, where one molecule stays static within an FtsZ-filament that is treadmilling for roughly 12 s (IU14288) to 17 s (IU15599; *SI Appendix*, Fig. S12) on average. (*C*) Histogram displaying the time an FtsZ-HT SM is bound within nonmature (nascent and equatorial) rings, mature septal rings, and combined from SM-TIRFm experiments performed on strain IU14352 (see *A*). Values are binned in 2.5-s increments. Labeled FtsZ-HT molecules that were present for 3 s or longer (at least three consecutive frames) were included in this analysis.

Treadmilling of FtsZ Filaments/Bundles in Mature and Nascent Rings and Dependence of FtsZ Filament Velocity on GTP Hydrolysis. Previous studies have shown that FtsZ filaments move by a treadmilling mechanism in *E. coli* and *B. subtilis* (12, 13). To demonstrate treadmilling of FtsZ filaments/bundles in *S. pneumoniae* mature and nascent rings (Fig. 1), we performed SM-TIRFm on two functional FtsZ-HT constructs, FtsZ-HT and iHT-FtsZ. A limiting concentration of HT substrate was added to approach SM detection of FtsZ-HT or iHT-FtsZ by TIRFm (40) (Fig. 4, red, and *SI Appendix*, Fig. S12) in cells whose outlines were delineated by bright-field microscopy. EzrA-mNG was used as a fiducial marker for the locations of rings (Fig. 4, green) in experiments using FtsZ-HT. As presented below, FtsZ and EzrA exhibit similar patterns of movement in nascent and mature rings. In mature septal, nascent, and equatorial rings in daughter cells, SMs of FtsZ appear as stationary foci that persist before disappearing (Fig. 4A, red spots, *SI Appendix*, Fig. S12C, and Movie S4). We interpret these transient, static foci of single FtsZ molecules as representing nonmoving FtsZ molecules within the cores of FtsZ filaments/bundles that are translocating by a treadmilling mechanism (Fig. 4B). The average lifetime of FtsZ-HT foci detected in mature and nascent rings was 11.9 ± 9.1 s, with some foci persisting for 15–20 s in the strain also expressing EzrA-mNG (Fig. 4C). The average lifetime of FtsZ-HT in the absence of EzrA-mNG, or of iHT-FtsZ was 12.7 ± 8.5 s or 16.8 ± 11.7 s, respectively (*SI Appendix*, Fig. S12A). The average length of a treadmilling filament is set by the subunit lifetime and average filament speed, because subunits bind to the plus end of a filament, and then depolymerize from the minus end (Fig. 4B). Thus, the estimated FtsZ filament length is 519 ± 399 nm for FtsZ-HT or 506 ± 420 nm for iHT-FtsZ (*SI Appendix*, Fig. S12B). This length is larger than the *E. coli* FtsZ filament cluster length determined by fluorescence microscopy in *E. coli* cells (41, 42), but matches the average *S. pneumoniae* FtsZ filament length reconstituted in-vitro (43).

In addition, we confirmed that the velocity of *S. pneumoniae* FtsZ filament/bundle movement depends on GTP hydrolysis by FtsZ, as reported previously for other bacteria and in biochemical

reactions (12, 13, 43). For these experiments, we constructed a *S. pneumoniae* mutant expressing FtsZ(G107S), which likely is defective in GTP binding based on homologs in other bacteria (*SI Appendix*, Fig. S13*A*) (44). The *ftsZ*(G107S) mutant is temperature-sensitive for growth and lyses at 42 °C (*SI Appendix*, Fig. S13*B*). Following a shift from 32 °C to 42 °C, the *ftsZ*(G107S) mutant formed larger, more spherical cells than the *ftsZ*⁺ parent strain, although the relative cellular amount of FtsZ(G107S) was comparable to that of FtsZ⁺ in cells at 42 °C (*SI Appendix*, Fig. S13 *C–E*). Strains expressing FtsZ(G107S)-sfGFP are not viable. Therefore, we constructed a *ftsZ*(G107S)//*bgaA*::P$_{Zn}$-*ftsZ-sfgfp* merodiploid strain in which we expressed and tracked the movement of low levels of ectopically expressed FtsZ-sfGFP by adding limited concentrations (0.1/0.01 mM) of Zn²⁺/Mn²⁺ at the still-permissive temperature of 37 °C (*SI Appendix*, Fig. S14). Under these conditions, the *ftsZ*⁺//P$_{Zn}$-*ftsZ-sfgfp* and *ftsZ*(G107S)//P$_{Zn}$-*ftsZ-sfgfp* strains show overall similar growth and FtsZ-sfGFP localization (*SI Appendix*, Fig. S14), although slightly aberrant cells with mislocalized FtsZ-sfGFP were occasionally observed for the *ftsZ*(G107S)//P$_{Zn}$-*ftsZ-sfgfp* strain. TIRFm of nascent FtsZ rings revealed that FtsZ-sfGFP filaments still move bidirectionally, but with significantly reduced velocity in the *ftsZ*(G107S) mutant compared with the *ftsZ*⁺ parent strain (*SI Appendix*, Fig. S15 and Movie S5). Overexpression of another mutant allele, FtsZ (D214A) that is defective in GTPase activity, also severely decreases FtsZ filament/bundle velocity (see below) (*SI Appendix*, Figs. S24*A* and S25 *A* and *B*). We conclude that *S. pneumoniae* FtsZ filament/bundle velocity produced by treadmilling is dependent on GTP binding and hydrolysis by FtsZ, consistent with previous studies in other bacteria (12, 13, 16).

FtsA and EzrA Form Nascent Rings with FtsZ in *S. pneumoniae*. We examined the movement of several proteins involved in FtsZ filament formation and stabilization (FtsA and EzrA) and in septal PG synthesis and cell division (MapZ, GpsB, MltG, DivIVA, StkP, bPBP2x, and FtsW) (see Introduction). Of this set, only FtsA and EzrA localize with FtsZ throughout the *S. pneumoniae* cell cycle (*SI Appendix*, Fig. S4 *B–F*) and form nascent rings in early divisional cells (Fig. 5 and Movies S6 and S7). In summations of TIRFm movies, FtsZ, FtsA, and EzrA localize distinctly in mature septal, nascent, and equatorial rings and are not detected elsewhere in *S. pneumoniae* cells (Fig. 5 *A* and *B*). Kymographs along the long axis of cells show outward movement of EzrA and FtsA rings over a 9-min period, similar to that of FtsZ filaments (Fig. 2 and *SI Appendix*, Fig. S16). Kymographs along the nascent and equatorial ring planes revealed that EzrA and FtsA traverse circumferentially, similarly to FtsZ (Fig. 5). The average velocity of EzrA-mNG (29.6 ± 15.3 nm/s), EzrA-GFP (33.6 ± 14.3 nm/s), and GFP-FtsA (33.3 ± 12.7 nm/s) in nascent/equatorial rings was similar to that of FtsZ filaments (Fig. 5*C* and *SI Appendix*, Fig. S17*C*). Another sandwich-fusion construct of FtsA (FtsA′-sfGFP-FtsA′) consistently moved ~31% faster (41.7 ± 16.2 nm/s) than most FtsZ or EzrA fusions in nascent rings (*SI Appendix*, Figs. S9*B* and S17 *B* and *C*). As noted above, an FtsZ-HT fusion also moved ~28% faster than three other FtsZ fusion constructs (*SI Appendix*, Fig. S9*B*). Overall, six FtsZ, EzrA, and FtsA fusions moved with approximately the same velocity of ~32 nm/s, suggesting that the slightly faster velocity of the FtsZ-HT and FtsA′-sfGFP-FtsA′ constructs is anomalous. We conclude that FtsA and EzrA proteins associate with and stabilize FtsZ filaments throughout the *S. pneumoniae* cell cycle and have similar overall dynamics as FtsZ filaments/bundles, including nascent ring formation.

MapZ Location Corresponds to Positions of Nascent FtsZ and EzrA Rings in Early Divisional *S. pneumoniae* Cells. We wondered whether nascent ring formation of FtsZ, FtsA, and EzrA was coincident with movement of MapZ protein rings, which emerge from either side of mature septal rings concomitant with the start of peripheral PG synthesis (*SI Appendix*, Fig. S1*A*) and move perpendicular to the long axis of cells to the equators of the new daughter cells
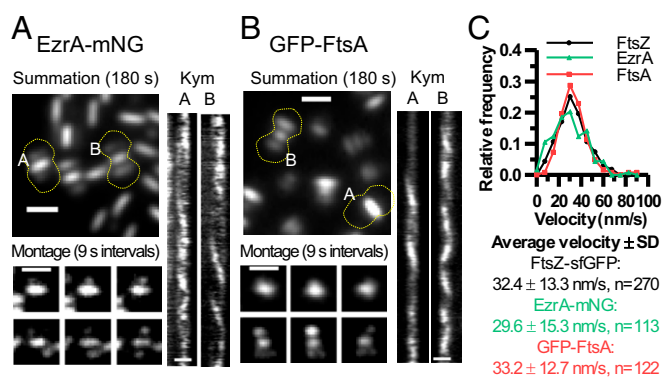

Fig. 5. Similar movement of EzrA, FtsA, and FtsZ filaments in nascent and early equatorial rings. Movement of EzrA-mNG (IU14117) (*A*) or GFP-FtsA (IU10035) (*B*) were visualized by TIRFm on agarose pads as described in *SI Appendix, Experimental Procedures*. Summations are shown of individual frames of 180-s movies (at one frame per second; Movies S6 and S7). The dotted lines are approximate outlines of cell shape. Montages of snapshot images show movement at 9-s intervals for nascent or early equatorial rings labeled "A" and "B" in the summations. Kymographs of the movement of EzrA-mNG or GFP-FtsA in these rings over 180 s are shown. (Scale bars, 1.0 μm.) (*C*) Distributions of velocities of FtsZ-sfGFP (IU9985; *n* = 270), EzrA-mNG (IU14117; *n* = 113), and GFP-FtsA (IU10035; *n* = 122) in nascent and early equatorial rings from two to four independent biological replicates. Values are binned in increments of 7.5 nm/s. No significant difference between velocities in *C* was indicated by one-way ANOVA analysis (GraphPad Prism, nonparametric Kruskal–Wallis test).

(*SI Appendix*, Figs. S1*B* and S18) (26, 27). In demographs and summations of movies, MapZ is localized primarily in mature septa or in two rings adjacent to septa, although a slight haze of MapZ remains between equatorial rings until FtsZ had fully exited from septa (*SI Appendix*, Figs. S4*A* and S18*C* and Movie S8). No directional movement of MapZ or fluctuations of MapZ signal was observed in rings in kymographs (*SI Appendix*, Fig. S18 *C* and *D*), consistent with minimal MapZ movement reported previously for *S. mutans* MapZ (33). This conclusion was confirmed directly by SM-TIRFm of iHT-MapZ, which unlike HT-MapZ, did not cause cell morphology defects (*SI Appendix*, Fig. S18 *A* and *B*). SMs of iHT-MapZ that appeared in MapZ rings remained static for as long 60 s to >100 s before disappearing due to motion out of the TIRF plane or photobleaching (*SI Appendix*, Fig. S18 *E* and *F* and Movie S9).

In high-resolution 3D-structured illumination microscopy (SIM) images of cells coexpressing tagged MapZ and FtsZ, low amounts of FtsZ are detected in early divisional cells at positions corresponding to nascent rings observed by TIRFm (Fig. 1; arrowhead in Fig. 6 *A*, *i* and *ii*). These nascent FtsZ rings overlap with MapZ rings moving away from septa. Similarly, EzrA in nascent rings overlaps with the parallel MapZ rings adjacent to the septum in early divisional cells (dotted box, Fig. 6*A*, *iii*). In later divisional cells, EzrA remains at constricting septa surrounding segregating nucleoids, when all MapZ has moved to the equators of daughter cells, which also contain some EzrA (box, Fig. 6*A*, *iv*). These results are consistent with MapZ acting as a guide for the nascent rings of FtsZ, FtsA, and EzrA that initially delivers some, but not all, of FtsZ, FtsA, and EzrA to the equators of daughter *S. pneumoniae* cells.

If MapZ is a guide for formation of nascent rings, then we would expect aberrant movement of FtsZ/FtsA/EzrA filaments in Δ*mapZ* mutants. In the D39 *S. pneumoniae* genetic background, Δ*mapZ* mutants are viable and form nearly normal looking cells with some distortions and frequent misaligned division planes (23, 27, 45). However, some FtsZ-fusion constructs in Δ*mapZ* mutants exhibit a severe synthetic defect in growth and morphology that precludes their study in *S. pneumoniae* (23), but that was not commented upon in *S. mutans* (33). In contrast, FtsZ-sfGFP
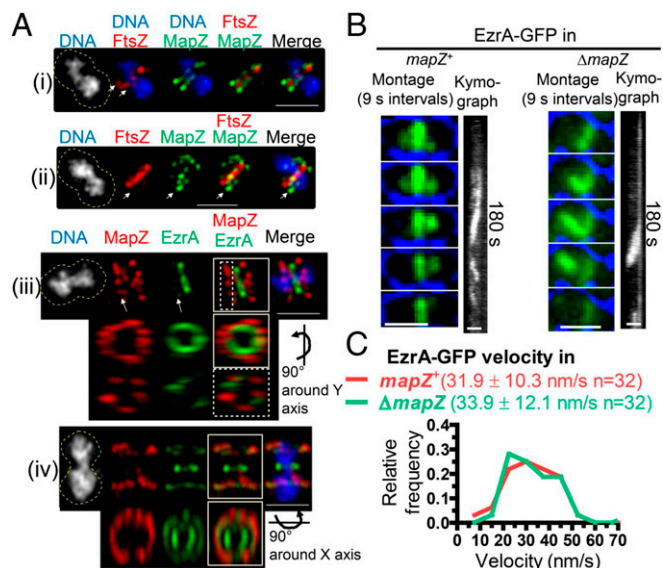
Fig. 6. MapZ is present in nascent ring planes containing FtsZ and EzrA filaments. IFM (*A*) or TIRFm (*B* and *C*) was performed to characterize the role of MapZ relative to FtsZ/EzrA filament organization. (Scale bars, 1 μm.) (*A*) Representative images of 3D-SIM dual IFM colocalizing FtsZ-Myc and MapZ-L-FLAG[3] (strain IU9090; *i* and *ii*) or MapZ-L-FLAG[3] and EzrA-HA (strain IU9207; *iii* and *iv*). Cultures were grown in BHI, at 37 °C in 5% CO_2, and IFM and DNA staining with DAPI were carried out as described in *SI Appendix, Experimental Procedures*. The dotted yellow lines in the DAPI column are approximate outlines of cell shape. For cells (*i*), (*ii*), and (*iii*), arrows point to the nascent ring plane where FtsZ or EzrA filaments can be seen. For cell (*iii*), the nascent ring (dotted box) and whole cell (solid box) were rotated, while for cell (*iv*), only the whole cell was rotated (solid box). The experiment was performed twice with similar results. (*B*) Representative montages and accompanying kymographs of EzrA-GFP (green in montage) overlaid with bright field (blue outline, cells are black) in *mapZ*+ (IU10449) versus Δ*mapZ* (IU10540), strains visualized by TIRFm (at one frame per second; see Movie S10). (Scale bars, 1 μm.) (*C*) No significant difference in the distributions of velocities of EzrA-GFP in the *mapZ*+ or Δ*mapZ* strains was found by an unpaired two-tailed *t* test (GraphPad Prism).

and EzrA-GFP fusions in Δ*mapZ* mutants lack this severe defect and appear similar to Δ*mapZ* mutants (Fig. 6*B* and *SI Appendix*, Fig. S9*C*). TIRFm of EzrA-GFP movement in a Δ*mapZ* mutant indeed revealed aberrant, untimed streaming of EzrA, presumably in association with FtsZ filaments, from parent to daughter cells, often resulting in rings that are not perpendicular to the long axis of cells (Fig. 6*B* and Movie S10). Nevertheless, the rate of EzrA streaming was similar in Δ*mapZ* and *mapZ*+ strains (Fig. 6*C*). Altogether, these results are consistent with MapZ acting as a continuous guide for the orderly movement of FtsZ/FtsA/EzrA filaments from mature septal rings to new equatorial rings in daughter cells. However, in the absence of MapZ, a second streaming mechanism aberrantly distributes FtsZ/FtsA/EzrA filaments into daughter cells.

bPBP2x Is Dynamic Compared with Other Proteins That Mediate PG Synthesis. We next examined the motion of several other proteins involved in PG synthesis in *S. pneumoniae*. GpsB (regulator), DivIVA (regulator), MltG (endo-lytic transglycosylase), StkP (Ser/Thr kinase), bPBP2x (TP), and FtsW (GT) (see Introduction) remain at mature septa until late in the division cycle after FtsZ, FtsA, and EzrA have largely moved to the equatorial rings of daughter cells (*SI Appendix*, Figs. S2*G* and S4 *G–L*). Unlike FtsZ, FtsA, and EzrA (Figs. 1, 2, and 5), TIRFm analysis did not detect GpsB, MltG, DivIVA, StkP, and bPBP2x joining nascent rings and showed that these proteins are largely confined to mature septal and equatorial rings (*SI Appendix*, Fig. S19, and Movies S11–S15; see also Fig. 8*A*). In these mature septal and equatorial rings, fluctuation of GpsB or MltG signal indicative of

ordered movement is not evident, whereas DivIVA and bPBP2x are actively moving, especially in equatorial rings (Fig. 7*A* and *SI Appendix*, Fig. S19 *A–C*), and bPBP2x motion is more diffusive around cells (Movie S15). In contrast, the motion of StkP is distinctively different from that of the other proteins examined. StkP locates in mature septal rings, where signal fluctuations are not readily apparent, but at the same time, StkP moves rapidly and diffusively throughout whole cells, which is captured as "clouds" of protein in summations of TIRFm movies (*SI Appendix*, Fig. S19*D* and Movie S14). Cells expressing GFP-StkP or HT-bPBP2x did not show obvious defects in growth or cell morphology (*SI Appendix*, Fig. S2), whereas HT-bPBP2x was labeled by an excess of HT-JF549 substrate. We conclude that of this set of proteins, only FtsZ and its ring stabilizers, FtsA and EzrA, form nascent rings and that dynamics of the other proteins varies from minimally detectable by TIRFm to diffusive.

bPBP2x and Its Partner FtsW Move at the Same Velocities Along Septal Rings. SM-TIRFm experiments were performed to delineate the motion of bPBP2x relative to FtsZ in mature septal rings (Fig. 7*B* and Movie S16). SM-TIRFm detection of HT-bPBP2x was approximated by addition of a limited amount of HT-JF549 substrate (Fig. 7*B*, red) that gave the same rate of bPBP2x movement when titrated downward to where labeled cells were barely detectable. FtsZ-sfGFP (Fig. 7*B*, green) and midcells determined from cell outlines (Fig. 7*B*, blue) were used as fiducial markers for the location of mature septal rings (Fig. 7*A*). Some bPBP2x molecules are detected as moving rapidly around cells in a sporadic fashion (Movie S16), consistent with TIRFm. The movement of these diffusive bPBP2x molecules was not analyzed further due to their lack of continuous tracks in SM-TIRFm. Other bPBP2x molecules attach onto mature septal rings and move directionally for at least 18 s (montage in Fig. 7*B*) and in some cases >30 s. The velocity of bPBP2x molecules in septal rings (21.9 ± 12.8 nm/s) is significantly slower than that of treadmilling by FtsZ filaments/bundles (32.4 ± 13.3 nm/s) (Fig. 7*C*). Control experiments showed that the velocity of SMs of HT-bPBP2x is the same in strains that express FtsZ-sfGFP (Fig. 7*C*) or that express FtsZ+ (Fig. 7*F*).

To further demonstrate that the velocity of HT-bPBP2x is not dependent on the fusion construct, we tracked the dynamics of FtsW-HT in *S. pneumoniae* (Fig. 7*F*, *SI Appendix*, Fig. S20, and Movie S17). New results demonstrate that the biochemical GT activity of FtsW depends on its interaction with its cognate class B PBP (46). We confirmed this interaction in *S. pneumoniae* cells by: (*i*) colocalization of FtsW and bPBP2x as part of the septal synthesis complex (Fig. 7*D*; demographs in *SI Appendix*, Fig. S2*G* and quantification of paired widths in *SI Appendix*, Fig. S2*H*) and (*ii*) by coimmunoprecipitation (co-IP) of FtsW with bPBP2x as bait in a 1:1 complex based on molecular mass (Fig. 7*E*). Consistent with a bPBP2x:FtsW complex, HT-bPBP2x and FtsW-HT move along mature septal rings at the same velocity in SM-TIRFm (Fig. 7*F*, *SI Appendix*, Fig. S20 *A* and *B*, and Movie S16), which is slower than that of FtsZ treadmilling. In addition, both proteins display some level of sporadic movement throughout the membrane in TIRFm summations (Fig. 7*A* and *SI Appendix*, Fig. S20*C*), suggesting that their interaction may occur independently of divisome localization. Attempts to determine the velocity of FtsW-GFP by TIRFm (*SI Appendix*, Fig. S20*D*) and compare it with that of FtsW-HT (Fig. 7*F* and *SI Appendix*, Fig. S20 *B* and *C*) were not successful. Unlike FtsW-HT at septa after ~2 h of saturated labeling (*SI Appendix*, Fig. S20*C*), the density of FtsW-GFP was too dense at septa to distinguish circumferential velocities in TIRFm kymographs.

Movement of bPBP2x and FtsW Depends on PG Synthesis and Not FtsZ Treadmilling in *S. pneumoniae*. Finally, we examined whether the velocity of bPBP2x and FtsW is strongly correlated with FtsZ treadmilling, as was demonstrated in *E. coli* and *B. subtilis* (12, 13). We found that there is minimal correlation between the velocity of bPBP2x movement on septa and the rate of FtsZ
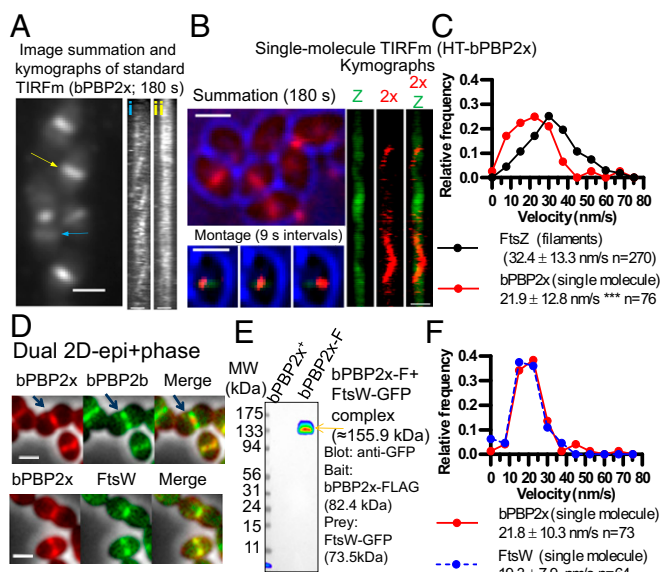
Fig. 7. bPBP2x and FtsW septal PG synthesis enzymes colocalize, interact, and show the same movement dynamics in *S. pneumoniae* cells. Microscopy experiments were performed in C+Y pH 6.9–7.1, while Co-IP was performed in BHI as described in *SI Appendix, Experimental Procedures*. (*A*) Dynamic movement of multiple HT-bPBP2x molecules in strain IU13910 labeled with a relatively high concentration (0.5 μM) of HT-JF549 ligand for 15 m and washed before imaging (Movie S15). Summation (1–180 s, at one frame per second) with kymographs corresponding to the rings marked by colored arrows [blue (*i*) or yellow (*ii*)]. (Scale bars, 1.0 μm.) (*B*) Dynamics of SMs of HT-bPBP2x in strain IU14103 expressing FtsZ-sfGFP. Cells were labeled with a limited amount (120 pM HT-JF549 ligand), washed, and SM-TIRFm of HT-bPBP2x was performed as described in *SI Appendix, Experimental Procedures* (Movie S16). Summation of individual frames from 180-s TIRFm movie showing bright-field (blue) outlines of cells and HT-bPBP2x (red). Montage of a series of frames at 9-s intervals corresponding to the white arrow in the summation showing a HT-bPBP2x molecule (red) moving on a mature FtsZ septal ring (green) in the middle of a cell (blue). The 180-s kymographs for FtsZ (Z), bPBP2x (2x), and merged FtsZ/bPBP2x correspond to the white arrow in the summation. (Scale bars, 1.0 μm.) (*C*) Distributions of velocities of FtsZ-filaments/bundles (*n* = 270) and SMs of bPBP2x (*n* = 76). Values are binned in intervals of 7.5 nm/s. FtsZ velocities are taken from Fig. 1*D* for filaments/ bundles in nascent and early equatorial rings, whereas bPBP2x velocities are taken from directionally moving SMs in mature septal FtsZ rings, such as those shown in *B*. Data are from two independent biological replicates. (*D*) Representative 2D-epifluorescence microscopy overlaid with phase-contrast images demonstrates colocalization of FtsW-GFP and iHT-bPBP2x to the inner septal ring in strain IU15066 (*Lower*), whereas sfGFP-bPBP2b localizes adjacent to iHT-bPBP2x inner rings in strain IU15068 (*Upper*). Arrows indicate iHT-bPBP2x (red) interior to sfGFP-bPBP2b (green). Cells were labeled with HT-TMR ligand as described in *SI Appendix, Experimental Procedures*, and the experiment was performed twice with similar results. (Scale bars, 1 μm.) (*E*) FtsW-GFP (prey) is eluted with bPBP2x-FLAG (bait) in Co-IP from minimally cross-linked *S. pneumoniae* cells of strain IU14964 (right lane) compared with untagged control strain (IU8918; left lane). FtsW-GFP was detected using anti-GFP, and the band shown was also detected with anti-FLAG antibody, confirming the presence of bPBP2x-FLAG. The experiment was performed twice with similar results. (*F*) Distributions of velocities of SMs of HT-bPBP2x (strain IU13910) and FtsW-GFP (strain IU15096) labeled with 120 pM of HT-JF549 ligand (Movies S16 and S17). Values are binned in intervals of 7.5 nm/s. Data are from three to five independent biological replicates. See *SI Appendix*, Fig. S20 *A* and *B* for representative SM-TIRFm kymographs.

treadmilling (Fig. 8*A*). To perform these experiments, we determined the velocity of bPBP2x at septa by SM-TIRFm in FtsZ (GTPase) mutants that slowed down FtsZ treadmilling by ~2× [FtsZ(G107S)] (*SI Appendix*, Figs. S21 and S22 and Movie S18) or ~10× [overexpression of FtsZ(D214A)] (*SI Appendix*, Figs. S23–S25 and Movies S19 and S20) and that lead to a percentage of cells with aberrantly placed division rings. Strikingly, reduction

of FtsZ treadmilling velocity by ~2× or ~10× does not reduce bPBP2x velocity or reduces it only slightly (~1.3×), respectively (Fig. 8*A* and *SI Appendix*, Figs. S24 and S25*C*). Notably, in the FtsZ(D214A) mutant, bPBP2x moves ~5× faster than the FtsZ filaments/bundles. Similarly, FtsW velocity is reduced by only ~1.4× in the FtsZ(D214A) mutant (*SI Appendix*, Fig. S25*D*). Finally, reduction of FtsZ treadmilling velocity over this range does not affect the net level of PG synthesis, as determined by incorporation of FDAA label for 2.5 m (Fig. 8*B*). These results contrast sharply with those for *B. subtilis*, where inhibition of FtsZ treadmilling significantly reduces FDAA labeling (12).

We next tested whether bPBP2x:FtsW velocity depends on PG synthesis. In *S. pneumoniae*, there are two MurA (UDP-*N*-acetylglucosamine enolpyruvyl transferase) homologs that catalyze the first committed step of PG synthesis (47, 48). Deletion of *murA1* (*spd_0967*; also called *murZ*) does not significantly alter growth, cell morphology, or FtsZ treadmilling velocity in C+Y, pH 7.1 (*SI Appendix*, Fig. S26*C*). However, the velocity of bPBP2x and FtsW is consistently reduced by ~1.5× in the Δ*murA1* mutant compared with the *murA1*⁺ parent (Fig. 8*C*). We conclude that limitation of PG synthesis slows down bPBP2x:FtsW velocity without detectably affecting FtsZ filament/bundle velocity. Finally, we added the β-lactam methicillin at a concentration that inhibits most of bPBP2x TP activity almost specifically (22). Methicillin addition did not inhibit FtsZ treadmilling velocity (Movie S21), but nearly completely stopped the movement of bPBP2x (Fig. 8*D*, *SI Appendix*, Fig. S27, and Movie S22). Together, these combined results indicate that movement of bPBP2x:FtsW complexes along septal rings depends on PG synthesis and is independent of the movement of FtsZ filaments/bundles.

Discussion

Partitioning of FtsZ filaments/bundles into daughter cells occurs in ovoid-shaped (ovococcus) bacteria, such as *S. pneumoniae*, by a mechanism that is fundamentally different from the Min and nucleoid occlusion systems present in rod-shaped bacteria (49, 50). Early in division, a ring containing MapZ protein splits from and moves parallel to the initial septal ring toward the site of the new equators in the daughter cells (*SI Appendix*, Fig. S1). Movement of MapZ rings is presumably driven by outward peripheral PG synthesis from the midcell septum and is preceded by movement of the origin of replication during chromosome segregation, which is promoted by transcription and unknown mechanisms (23, 51). *S. pneumoniae* MapZ is a bitopic membrane protein, whose 40 amino-terminal amino acids of its cytoplasmic domain can bind to FtsZ and whose extracellular carboxyl-terminal domain binds to PG (26, 52). However, the amino-terminal FtsZ binding amino acids are not conserved in *S. mutans* MapZ (33). MapZ is phosphorylated by the StkP Ser/ Thr kinase; but, a requirement for MapZ phosphorylation on cell division and morphology seems to depend on the *S. pneumoniae* genetic background (26, 27). Similarly, in one laboratory strain, MapZ forms a third ring at division septa (26), whereas in other laboratory strains and in the progenitor D39 background of most laboratory strains, this third ring is rarely detected (*SI Appendix*, Figs. S2*C*, S4*A*, and S18*B*) (23, 27), making it unlikely that it plays an obligatory role in *S. pneumoniae* division.

The interesting conjecture was made that as MapZ reaches the equators of daughter cells, it serves as a "beacon" for relocalization of FtsZ from mature septal rings (26). A recent paper proposes a concerted streaming mechanism in which FtsZ moves late in division from septa to equators in some *S. mutans* cells (33). In contrast, here we report that FtsZ transport to equators in *S. pneumoniae* is a continuous process throughout the cell cycle (Fig. 9). Early in *S. pneumoniae* division, nascent filaments/ bundles of FtsZ are detected near and moving parallel to mature septal rings (Figs. 1 and 9). In the ~10-min interval (one-third of a generation) between the initial movement of MapZ and the migration of most FtsZ to equators (*SI Appendix*, Fig. S4 *A* and *B*), nascent FtsZ filaments/bundles move outward and become more dense until they reach equators, after which the remainder of FtsZ
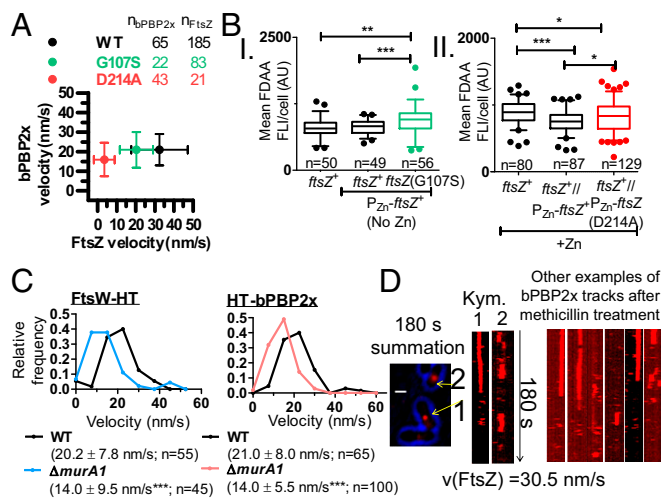
Fig. 8. *S. pneumoniae* bBPB2x and FtsW movement depend on PG synthesis and are not correlated with FtsZ treadmilling or FtsZ(GTPase) activity. Strains were grown in C+Y, pH 6.9 at 37 °C in 5% CO_2 to $OD_{620} = 0.1–0.2$, at which point cells were labeled with FDAA, washed, and fixed. Alternatively, cells were labeled with 120 pM HT-JF549 ligand, washed, and SM-TIRFm performed (at one frame per second) to track dynamics of HT-bPBP2x or FtsW-HT. (*A*) Mean HT-bPBP2x velocity is not correlated with FtsZ-sfGFP treadmilling velocity. Average velocities ± SDs from two or three independent biological replicates are shown for strains: IU9985 (*ftsZ-sfgfp*), IU13910 (*ht-pbp2x*), IU14375 [*ftsZ*(G107S) P_Zn-*ftsZ-sfgfp*], IU14508 [*ftsZ*(G107S) *ht-pbp2x*]; IU15181 [P_Zn-*ftsZ*(D214A) *ftsZ-sfgfp*], and IU15041 [P_Zn-*ftsZ*(D214A) *ht-pbp2x*] (*SI Appendix, Experimental Procedures* and Table S1 and Movies S5 and S18–S20). (*B*) Box-and-whisker plots (whiskers, 5th and 95th percentile) of different FtsZ(GTPase) mutants showing that mean FDAA labeling of PG per cell is not reduced in FtsZ(GTPase) merodiploid mutants (middle compared with right strains). *P* values were obtained by one-way ANOVA analysis (GraphPad Prism, nonparametric Kruskal–Wallis test, where *P < 0.05; **P < 0.01; ***P < 0.001). Values are from two independent biological replicates (*SI Appendix, Experimental Procedures*). (*C*) HT-bPBP2x and FtsW-HT velocity is reduced in the absence of MurA1. Velocities were determined by SM-TIRFm in strains IU13910 (*ht-pbp2x*), IU15039 (Δ*murA1 ht-pbp2x*), IU15096 (*ftsW-ht*), and IU15173 (Δ*murA1 ftsW-ht*) as described in Fig. 7. Shown is the average velocity ± SD of *n* tracks. *P* values were obtained by one-way unpaired, two-tailed *t* tests (GraphPad Prism), where ***P < 0.001. (*D*) HT-bPBP2x movement is inhibited when cells are treated with methicillin. A final methicillin concentration of 0.3 μg/mL was added on top of an agarose pad, after which IU13910 (*ht-pbp2x*) cells were added as described in *SI Appendix, Experimental Procedures*. Cells were visualized by SM-TIRFm after 45–75 m of treatment with methicillin at 37 °C (Movie S22). A summation is shown of movie frames over 180 s with arrows pointing at septa where molecules of bPBP2x no longer move circumferentially, as indicated by the kymographs (*n* = 57). (Scale bar, 1.0 μm.) Numbers correspond to the arrows in the summation. The experiment was performed independently twice with similar results. The velocity of FtsZ-sfGFP remained unchanged, consistent with FtsZ treadmilling, independent of PG synthesis (*n* = 84) (*SI Appendix,* Fig. S27 and Movie S21).

migrates to form mature equatorial rings (Fig. 2). Progressive nascent ring formation was detected in both Δ*cps* derivatives and in the progenitor encapsulated *cps*+ parent D39 strain. These nascent FtsZ rings also contain EzrA and FtsA, which bind to, membrane anchor, and stabilize FtsZ filaments/bundles (Fig. 5 and *SI Appendix,* Fig. S16), but none of the other PG synthesis proteins analyzed in this study was detected moving in nascent rings. FtsZ, FtsA, and EzrA move at the same velocity in the majority of tagged constructs (*Results*), indicative of formation of nascent FtsZ/FtsA/EzrA filament/bundle.

High-resolution microscopy and effects of a Δ*mapZ* mutation suggest that nascent FtsZ/FtsA/EzrA filaments/bundles use MapZ as a guide, as opposed to a beacon, to reach the equators of daughter cells. Three-dimensional SIM immunofluorescence microscopy (IFM) images detect FtsZ and EzrA together with

MapZ in early and later nascent rings (Fig. 6*A*). Furthermore, in the absence of MapZ, orderly nascent EzrA rings are lost, and EzrA abruptly streams between daughter cells, often resulting in the aberrant ring orientation reported previously (Fig. 6*B*) (23). Streaming rarely was observed in wild-type *S. pneumoniae* cells (~1%) and represents a second mechanism for translocation of FtsZ and its associated proteins to daughter cells. In this respect, streaming is a "failsafe" mechanism that accounts for the lack of lethality of *S. pneumoniae* Δ*mapZ* mutations.

In *S. mutans* cells, continuous FtsZ nascent ring formation was not reported and streaming, which was detected in ~7% of cells, is proposed as the primary mechanism for FtsZ movement from septal to equatorial rings (figure 6 in ref. 33). A possible reason for this difference is that *S. pneumoniae* and *S. mutans* are evolutionarily distant *Streptococcus* species (33), and ovococcus bacteria exhibit differences in the relative timing of septal and peripheral PG synthesis (53). On the other hand, technical or strain differences may underlie the different results. In particular, the *S. mutans* cells in movies shown in ref. 33 appear to be in middle-to-late divisional stages and contain prominent equatorial rings, whereas movement of *S. pneumoniae* FtsZ was recorded in early-to-late stages of division in this study (Figs. 1 and 2). Taken together, our results indicate that treadmilling FtsZ/FtsA/EzrA filaments/bundles are components of migrating MapZ rings throughout the cell cycle in *S. pneumoniae* (Fig. 9), and may thus play an important role in assembly and organization of these rings, about which little is known. This transport mechanism also moves part of the cellular FtsZ population to
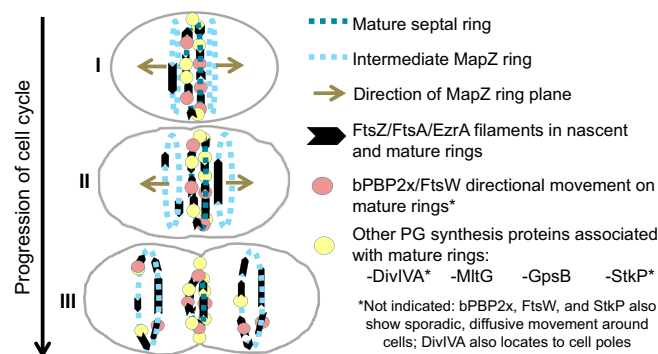
Fig. 9. Summary diagram of the movement dynamics of FtsZ, FtsA, EzrA, bPBP2x, FtsW, and regulators of PG synthesis in *S. pneumoniae* cells. The division cycle is simplified to three stages. In early divisional cells (I), the equator becomes the septum of dividing cells, and most divisome proteins locate to the mature septum, with the exception of StkP and bPBP2x, which also exhibit sporadic, diffusive movement throughout cells. bPBP2x and FtsW molecules attach to the mature septal ring and move in one direction or the other for as long as 30 s. After the start of peripheral PG synthesis, MapZ bifurcates into rings on both sides of the mature septal ring, and the MapZ rings start to move outward toward the positions of the equators in the daughter cells (I–II). Concurrently, nascent filaments/bundles consisting of FtsZ and its associated proteins FtsA and EzrA are detected in MapZ rings, suggesting that MapZ rings continuously guide a fraction of FtsZ/FtsA/EzrA to new equatorial rings, where FtsZ may nucleate the transport of remaining FtsZ from the mature septal ring later in division. Treadmilling velocity and dynamics of FtsZ and EzrA are the same in mature septal, nascent, and equatorial rings, whereas FtsA may move faster than FtsZ in nascent rings. FtsZ/FtsA/EzrA filaments/bundles accumulate as nascent MapZ rings move away from the mature septal ring and become early equatorial rings in daughter cells. Directional movement in or association with nascent rings was not detected for PG synthesis proteins bBPB2x, FtsW, DivIVA, MltG, StkP, and GpsB, and these PG synthesis proteins remain at constricting septa until migrating to new equatorial rings late in cell division, where bBPB2x and FtsW form a complex and move circumferentially in either direction (III). The movement of bPBP2x:FtsW complexes in septal PG synthesis depends on and reflects new PG synthesis and is not correlated with the treadmilling of FtsZ filaments/bundles. See *Discussion* for additional details.

the equatorial rings, where the FtsZ filaments/bundles may serve to nucleate the transport of the remainder of septal FtsZ later in the division cycle (Fig. 9). This movement likely occurs mainly by depolymerization of FtsZ filaments/bundles and possibly by some new protein synthesis, because concerted streaming of FtsZ filaments/bundles was rarely observed in wild-type *S. pneumoniae* cells.

In the course of these studies, we also determined a set of basic parameters about FtsZ dynamics in *S. pneumoniae* cells. Filaments/bundles of wild-type FtsZ always move with a velocity of ~32 nm/s in rings at all stages of division and while streaming in Δ*mapZ* mutants (Figs. 1*D*, 3*B*, and 6*C*). The same velocity of FtsZ filament/bundle movement was determined by TIRFm (Fig. 1*D*) and independently by wide-field observation of vertically immobilized cells (Fig. 3). A treadmilling mechanism of FtsZ filament/bundle movement was confirmed directly by SM-TIRFm (Fig. 4 and *SI Appendix*, Fig. S12). SM-TIRFm and immobilized cell measurements indicated the lifetime of FtsZ subunits in filaments/bundles is ~15 s (Fig. 4*C* and *SI Appendix*, Fig. S12) and the lifetime of entire FtsZ filaments/bundles is ~17 s (Fig. 3*D*). Based on the average subunit lifetime and the velocity of filament/bundle movement, the average length of treadmilling FtsZ filaments/bundles in *S. pneumoniae* cells is ~500 nm (*SI Appendix*, Fig. S12*B*), which is similar to the length of double-stranded *S. pneumoniae* FtsZ filaments reconstituted in vitro (43). In addition, our measurements show that the processivity of treadmilling of FtsZ filaments/bundle is ~500 nm (Fig. 3*C*), indicating that FtsZ filaments/bundles traverse ~20% of the circumference of *S. pneumoniae* cells on average. Finally, as expected from previous precedents (12, 13), mutations that decrease GTP binding or the GTPase activity of FtsZ reduce the velocity of FtsZ treadmilling by as much as 10× (Fig. 8*A*). FtsZ (GTPase) mutations also disrupt the placement of division planes compared with wild-type cells (*SI Appendix*, Figs. S14, S21, and S23).

Besides FtsZ, FtsA, and EzrA, none of the PG synthesis proteins tested in this study was a member of translocating MapZ rings (*SI Appendix*, Fig. S16). Within the limits of standard TIRFm, some of these proteins showed minimal movement in mature septal and equatorial rings (i.e., GpsB, MltG, and StkP) (Introduction and *SI Appendix*, Fig. S19), whereas DivIVA and bPBP2x showed obvious dynamic movements (Fig. 7*A* and *SI Appendix*, Fig. S19*C*). We therefore determined the role of FtsZ treadmilling on the motion of bPBP2x and its partner FtsW in mature septa of *S. pneumoniae* cells. A new biochemical study reports that FtsW GT activity depends on interactions with its cognate class B PBP (46). In support of this interaction in *S. pneumoniae* cells, bPBP2x and FtsW colocalize at all stages of *S. pneumoniae* division (Fig. 7*D* and *SI Appendix*, Fig. S2 *G* and *H*) and bPBP2x pulls down FtsW in a likely 1:1 complex (Fig. 7*E*). In addition, SM-TIRFm showed that bPBP2x and FtsW move at the same velocity on septa (Fig. 7*F*). Moreover, besides bPBP2x stimulating FtsW GT activity in *S. pneumoniae* cells, the TP activity of bPBP2x is required for septal PG synthesis, because a *pbp2x* (S337A) active-site mutant is not viable (54), resulting in elongated cells lacking septal closure (*SI Appendix*, Fig. S28). This result is consistent with the notion that both bPBP2x TP and FtsW GT activities are required to drive bPBP2x:FtsW movement in the septa of *S. pneumoniae* cells, as discussed next.

Five pieces of evidence support the conclusion that movement of the bPBP2x:FtsW complex in septa of *S. pneumoniae* cells depends on PG synthesis and not on FtsZ treadmilling. First, the velocity of bPBP2x and FtsW is slower than that of FtsZ treadmilling in wild-type *S. pneumoniae* cells (Fig. 7*C*). Second, the decreased velocity of FtsZ treadmilling in FtsZ(GTPase) mutants is not correlated with a decrease of bPBP2x velocity (Fig. 8*A*). In fact, in the slowest mutant [FtsZ(D214A) overexpression], bPBP2x is moving about 5× faster than FtsZ treadmilling. Third, severe reduction in FtsZ treadmilling velocity does not markedly decrease PG synthesis indicated by FDAA incorporation (Fig. 8*B*). Fourth, a decrease in PG synthesis precursors caused by a Δ*murA1* mutation,

decreases the velocity of bPBP2x and FtsW by the same amount, but does not decrease FtsZ treadmilling rate (Fig. 8*C*). Finally, addition of methicillin at a concentration that mainly inhibits bPBP2x TP activity stops the movement of bPBP2x, but does not decrease the velocity of FtsZ treadmilling (Fig. 8*D*).

These results strongly support the conclusion that the movement of the bPBP2x:FtsW complex in septal PG synthesis in *S. pneumoniae* cells depends on and likely mirrors new PG synthesis and is not correlated with the treadmilling of FtsZ filaments/bundles. In contrast, the velocities of the septal class B PBPs of *B. subtilis* and *E. coli* are coupled to and limited by FtsZ treadmilling, resulting in a correlation between septal bPBP and FtsZ treadmilling velocities (12, 13). The mechanisms underlying this coupling and its relationship to the rate of PG synthesis in *B. subtilis* and *E. coli* are not understood. On the one hand, FtsZ treadmilling is further coupled to and limiting for septal PG synthesis and the constriction of *B. subtilis* cells (12). On the other hand, the velocity of FtsZ treadmilling is not correlated with the rate of PG synthesis determined by FDAA incorporation or the rate of septum closure of *E. coli* cells (13, 41). These differences suggest that additional metabolic (e.g., PG precursor pools) and structural (e.g., PG width and outer membrane synthesis) constraints may influence the relative rates of FtsZ treadmilling, bPBP complex movement, and PG synthesis in different bacteria (55, 56).

Besides the sidewall rod complexes of rod-shaped bacteria (14), there is another precedent for the dependence of PBP movement on PG synthesis. Recent results show that septal PG synthesis continues to close division septa of *S. aureus* after FtsZ treadmilling is inhibited by addition of a drug (PC190723) (16). This finding is again consistent with an FtsZ treadmilling-independent mechanism by which PG synthesis itself drives for PBP motion (13, 41). Attempts to perform a similar experiment with *S. pneumoniae* were not successful, because *S. pneumoniae* is not inhibited by PC190723 (57). The dependence of bPBP2x:FtsW movement on PG synthesis can be rationalized by a model proposed for the dependence of PBP movement on PG synthesis in sidewall elongation of rod-shaped bacteria (14). It was proposed that MreB filaments form tracks that direct the linear motion of PBP complexes (14, 58). At any point in a track, the PBP complex has used substrate behind it to synthesize PG, and the utilization of available substrate in front of it drives its motion. In the case of *S. pneumoniae* bPBP2x:FtsW, it is possible that FtsZ filaments/bundles, or other proteins in septal FtsZ rings, provide tracks that couple movement to PG synthesis. In this model, FtsZ treadmilling acts to dynamically distribute filament tracks that allow the spatial organization of directional PG synthesis, possibly through indirect interactions, as suggested recently for *E. coli* FtsZ and FtsN by high-resolution microscopy (42). Future studies will test this and related models to provide an understanding about the relationships among FtsZ treadmilling, PBP complex movement, and PG synthesis rate and location in different bacteria.

Experimental Procedures

Detailed experimental procedures are described in *SI Appendix, Experimental Procedures*, including: bacterial strains and growth conditions; Western blotting; 2D-epifluorescence microscopy and demograph generation; growth and imaging of live cells by TIRFm; TIRFm image acquisition and processing; periodicity analysis of FtsZ filaments/bundles in nascent rings; culture growth and sample preparation for microhole immobilization of *S. pneumoniae* cells; image acquisition, processing, and data analysis of vertically oriented cells in microholes; SM TIRFm; TIRFm of *ftsZ*(G107S)//P_{Zn}-*ftsZ*-*sfgfp* merodiploid strains; TIRFm of HT-bPBP2x in an *ftsZ*(G107S) mutant; TIRFm of P_{Zn}-*ftsZ*(D214A) or P_{Zn}-*ftsZ* (D214A)-*sfgfp* merodiploid strains; 3D-SIM IFM; co-IP of FtsW-GFP with bPBP2x-FLAG; labeling of FtsZ(GTPase) mutant cells with FDAAs; and TIRFm of methicillin-treated cells.

MICROBIOLOGY

1. Haeusser DP, Margolin W (2016) Splitsville: Structural and functional insights into the dynamic bacterial Z ring. *Nat Rev Microbiol* 14:305–319.
2. den Blaauwen T, Hamoen LW, Levin PA (2017) The divisome at 25: The road ahead. *Curr Opin Microbiol* 36:85–94.
3. Du S, Lutkenhaus J (2017) Assembly and activation of the *Escherichia coli* divisome. *Mol Microbiol* 105:177–187.
4. Coltharp C, Xiao J (2017) Beyond force generation: Why is a dynamic ring of FtsZ polymers essential for bacterial cytokinesis? *BioEssays* 39:1–11.
5. Meeske AJ, et al. (2016) SEDS proteins are a widespread family of bacterial cell wall polymerases. *Nature* 537:634–638.
6. Sham LT, et al. (2014) Bacterial cell wall. MurJ is the flippase of lipid-linked precursors for peptidoglycan biogenesis. *Science* 345:220–222.
7. Daniel RA, Harry EJ, Errington J (2000) Role of penicillin-binding protein PBP 2B in assembly and functioning of the division machinery of *Bacillus subtilis*. *Mol Microbiol* 35:299–311.
8. Du S, Pichoff S, Lutkenhaus J (2016) FtsEX acts on FtsA to regulate divisome assembly and activity. *Proc Natl Acad Sci USA* 113:E5052–E5061.
9. Gamba P, Veening JW, Saunders NJ, Hamoen LW, Daniel RA (2009) Two-step assembly dynamics of the *Bacillus subtilis* divisome. *J Bacteriol* 191:4186–4194.
10. Yao Q, et al. (2017) Short FtsZ filaments can drive asymmetric cell envelope constriction at the onset of bacterial cytokinesis. *EMBO J* 36:1577–1589.
11. Loose M, Mitchison TJ (2014) The bacterial cell division proteins FtsA and FtsZ self-organize into dynamic cytoskeletal patterns. *Nat Cell Biol* 16:38–46.
12. Bisson-Filho AW, et al. (2017) Treadmilling by FtsZ filaments drives peptidoglycan synthesis and bacterial cell division. *Science* 355:739–743.
13. Yang X, et al. (2017) GTPase activity-coupled treadmilling of the bacterial tubulin FtsZ organizes septal cell wall synthesis. *Science* 355:744–747.
14. Garner EC, et al. (2011) Coupled, circumferential motions of the cell wall synthesis machinery and MreB filaments in *B. subtilis*. *Science* 333:222–225.
15. Lee TK, et al. (2014) A dynamically assembled cell wall synthesis machinery buffers cell growth. *Proc Natl Acad Sci USA* 111:4554–4559.
16. Monteiro JM, et al. (2018) Peptidoglycan synthesis drives an FtsZ-treadmilling-independent step of cytokinesis. *Nature* 554:528–532.
17. Massidda O, Nováková L, Vollmer W (2013) From models to pathogens: How much have we learned about *Streptococcus pneumoniae* cell division? *Environ Microbiol* 15:3133–3157.
18. Garcia PS, Simorre JP, Brochier-Armanet C, Grangeasse C (2016) Cell division of *Streptococcus pneumoniae*: Think positive! *Curr Opin Microbiol* 34:18–23.
19. Morlot C, Zapun A, Dideberg O, Vernet T (2003) Growth and division of *Streptococcus pneumoniae*: Localization of the high molecular weight penicillin-binding proteins during the cell cycle. *Mol Microbiol* 50:845–855.
20. Mura A, et al. (2017) Roles of the essential protein FtsA in cell growth and division in *Streptococcus pneumoniae*. *J Bacteriol* 199:e00608–e00616.
21. Morlot C, Noirclerc-Savoye M, Zapun A, Dideberg O, Vernet T (2004) The D,D-carboxypeptidase PBP3 organizes the division process of *Streptococcus pneumoniae*. *Mol Microbiol* 51:1641–1648.
22. Land AD, et al. (2013) Requirement of essential Pbp2x and GpsB for septal ring closure in *Streptococcus pneumoniae* D39. *Mol Microbiol* 90:939–955.
23. van Raaphorst R, Kjos M, Veening JW (2017) Chromosome segregation drives division site selection in *Streptococcus pneumoniae*. *Proc Natl Acad Sci USA* 114:E5959–E5968.
24. Jacq M, et al. (2015) Remodeling of the Z-ring nanostructure during the *Streptococcus pneumoniae* cell cycle revealed by photoactivated localization microscopy. *MBio* 6:e01108–e01115.
25. Tsui HT, et al. (2014) Pbp2x localizes separately from Pbp2b and other peptidoglycan synthesis proteins during later stages of cell division of *Streptococcus pneumoniae* D39. *Mol Microbiol* 94:21–40.
26. Fleurie A, et al. (2014) MapZ marks the division sites and positions FtsZ rings in *Streptococcus pneumoniae*. *Nature* 516:259–262.
27. Holečková N, et al. (2014) LocZ is a new cell division protein involved in proper septum placement in *Streptococcus pneumoniae*. *MBio* 6:e01700–e01714.
28. Land AD, Luo Q, Levin PA (2014) Functional domain analysis of the cell division inhibitor EzrA. *PLoS One* 9:e102616.
29. Fadda D, et al. (2007) *Streptococcus pneumoniae* DivIVA: Localization and interactions in a MinCD-free context. *J Bacteriol* 189:1288–1298.
30. Tsui HC, et al. (2016) Suppression of a deletion mutation in the gene encoding essential PBP2b reveals a new lytic transglycosylase involved in peripheral peptidoglycan synthesis in *Streptococcus pneumoniae* D39. *Mol Microbiol* 100:1039–1065.
31. Rued BE, et al. (2017) Suppression and synthetic-lethal genetic relationships of Δ*gpsB* mutations indicate that GpsB mediates protein phosphorylation and penicillin-binding protein interactions in *Streptococcus pneumoniae* D39. *Mol Microbiol* 103:931–957.
32. Beilharz K, et al. (2012) Control of cell division in *Streptococcus pneumoniae* by the conserved Ser/Thr protein kinase StkP. *Proc Natl Acad Sci USA* 109:E905–E913.
33. Li Y, et al. (2018) MapZ Forms a stable ring structure that acts as a nanotrack for FtsZ treadmilling in *Streptococcus mutans*. *ACS Nano* 12:6137–6146.
34. Barendt SM, et al. (2009) Influences of capsule on cell shape and chain formation of wild-type and *pcsB* mutants of serotype 2 *Streptococcus pneumoniae*. *J Bacteriol* 191:3024–3040.
35. Ducret A, Quardokus EM, Brun YV (2016) MicrobeJ, a tool for high throughput bacterial cell detection and quantitative analysis. *Nat Microbiol* 1:16077.
36. Moreno-Gámez S, et al. (2017) Quorum sensing integrates environmental cues, cell density and cell history to control bacterial competence. *Nat Commun* 8:854.
37. Wilson M (2004) *Microbial Inhabitants of Humans: Their Ecology and Role in Health and Disease* (Cambridge Univ Press, Cambridge, UK).
38. Thanedar S, Margolin W (2004) FtsZ exhibits rapid movement and oscillation waves in helix-like patterns in *Escherichia coli*. *Curr Biol* 14:1167–1173.
39. Holden S (2018) Probing the mechanistic principles of bacterial cell division with super-resolution microscopy. *Curr Opin Microbiol* 43:84–91.
40. Grimm JB, et al. (2015) A general method to improve fluorophores for live-cell and single-molecule microscopy. *Nat Methods* 12:244–250.
41. Coltharp C, Buss J, Plumer TM, Xiao J (2016) Defining the rate-limiting processes of bacterial cytokinesis. *Proc Natl Acad Sci USA* 113:E1044–E1053.
42. Söderström B, Chan H, Shilling PJ, Skoglund U, Daley DO (2018) Spatial separation of FtsZ and FtsN during cell division. *Mol Microbiol* 107:387–401.
43. Salvarelli E, et al. (2015) The cell division protein FtsZ from *Streptococcus pneumoniae* exhibits a GTPase activity delay. *J Biol Chem* 290:25081–25089.
44. Redick SD, Stricker J, Briscoe G, Erickson HP (2005) Mutants of FtsZ targeting the protofilament interface: Effects on cell division and GTPase activity. *J Bacteriol* 187:2727–2736.
45. Boersma MJ, et al. (2015) Minimal peptidoglycan (PG) turnover in wild-type and PG hydrolase and cell division mutants of *Streptococcus pneumoniae* D39 growing planktonically and in host-relevant biofilms. *J Bacteriol* 197:3472–3485.
46. Taguchi A, et al. (2018) FtsW is a peptidoglycan polymerase that is activated by its cognate penicillin-binding protein. bioRxiv, 10.1101/358663.
47. Du W, et al. (2000) Two active forms of UDP-N-acetylglucosamine enolpyruvyl transferase in Gram-positive bacteria. *J Bacteriol* 182:4146–4152.
48. Slager J, Aprianto R, Veening JW (2018) Deep genome annotation of the opportunistic human pathogen *Streptococcus pneumoniae* D39. *Nucleic Acids Res* 46:9971–9989.
49. Rowlett VW, Margolin W (2015) The Min system and other nucleoid-independent regulators of Z ring positioning. *Front Microbiol* 6:478.
50. Wu LJ, Errington J (2011) Nucleoid occlusion and bacterial cell division. *Nat Rev Microbiol* 10:8–12.
51. Kjos M, Veening JW (2014) Tracking of chromosome dynamics in live *Streptococcus pneumoniae* reveals that transcription promotes chromosome segregation. *Mol Microbiol* 91:1088–1105.
52. Manuse S, et al. (2016) Structure-function analysis of the extracellular domain of the pneumococcal cell division site positioning protein MapZ. *Nat Commun* 7:12071.
53. Wheeler R, Mesnage S, Boneca IG, Hobbs JK, Foster SJ (2011) Super-resolution microscopy reveals cell wall dynamics and peptidoglycan architecture in ovococcal bacteria. *Mol Microbiol* 82:1096–1109.
54. Peters K, et al. (2014) *Streptococcus pneumoniae* PBP2x mid-cell localization requires the C-terminal PASTA domains and is essential for cell shape maintenance. *Mol Microbiol* 92:733–755.
55. Harris LK, Theriot JA (2016) Relative rates of surface and volume synthesis set bacterial cell size. *Cell* 165:1479–1492.
56. Sperber AM, Herman JK (2017) Metabolism shapes the cell. *J Bacteriol* 199:e00039-17.
57. Haydon DJ, et al. (2008) An inhibitor of FtsZ with potent and selective anti-staphylococcal activity. *Science* 321:1673–1675.
58. Hussain S, et al. (2018) MreB filaments align along greatest principal membrane curvature to orient cell wall synthesis. *eLife* 7:e32471.